Floquet engineering the band structure of materials with optimal control theory

Alberto Castro [1,2,*], Umberto De Giovannini,[3,4,†] Shunsuke A. Sato [5,4,‡] Hannes Hübener [4,§] and Angel Rubio[4,6,‖]

[1]*Institute for Biocomputation and Physics of Complex Systems, University of Zaragoza, 50018 Zaragoza, Spain*
[2]*ARAID Foundation, 50018 Zaragoza, Spain*
[3]*Università degli Studi di Palermo, Dipartimento di Fisica e ChimicaEmilio Segrè, via Archirafi 36, I-90123 Palermo, Italy*
[4]*Max Planck Institute for the Structure and Dynamics of Matter and Center for Free Electron Laser Science, 22761 Hamburg, Germany*
[5]*Center for Computational Sciences, University of Tsukuba, Tsukuba 305-8577, Japan*
[6]*Center for Computational Quantum Physics (CCQ), The Flatiron Institute, 162 Fifth avenue, New York, New York 10010, USA*

We demonstrate that the electronic structure of a material can be deformed into Floquet pseudobands with arbitrarily tailored shapes. We achieve this goal with a combination of quantum optimal control theory and Floquet engineering. The power and versatility of this framework is demonstrated here by utilizing the independent-electron tight-binding description of the π electronic system of graphene. We show several prototype examples focusing on the region around the K (Dirac) point of the Brillouin zone: creation of a gap with opposing flat valence and conduction bands, creation of a gap with opposing concave symmetric valence and conduction bands (which would correspond to a material with an effective negative electron-hole mass), and closure of the gap when departing from a modified graphene model with a nonzero field-free gap. We employ time-periodic drives with several frequency components and polarizations, in contrast to the usual monochromatic fields, and use control theory to find the amplitudes of each component that optimize the shape of the bands as desired. In addition, we use quantum control methods to find realistic switch-on pulses that bring the material into the predefined stationary Floquet band structure, i.e., into a state in which the desired Floquet modes of the target bands are fully occupied, so that they should remain stroboscopically stationary, with long lifetimes, when the weak periodic drives are started. Finally, we note that although we have focused on solid state materials, the technique that we propose could be equally used for the Floquet engineering of ultracold atoms in optical lattices and for other nonequilibrium dynamical and correlated systems.

I. INTRODUCTION

The possibility of preparing materials in nonequilibrium steady states with tailored properties by exciting them with continuous lasers and thereby manipulating—even designing—their electronic band structure has attracted considerable experimental and theoretical interest. Floquet theory maps the time dependence of any periodically driven system into a structure of states in energy space that are observable as replica bands in time-resolved angle-resolved photoemission spectroscopy (ARPES) [1–3]. A number of theoretical works [4–8] have proposed interpreting these dressed states or sidebands of such laser-driven materials as new quasipar-

ticle levels and identify the nonequilibrium steady states with the eigenstates of the Floquet operator. It is thus possible to predict a variety of new properties of such driven material states by analyzing the Floquet eigenstates. This has led to the idea sometimes referred to as Floquet engineering: tailoring the material properties with a periodic drive, by manipulating the Floquet electronic band structure. In particular, the topology of electronic Floquet states has been discussed in many works. The paradigmatic example is graphene under circularly polarized irradiation, which has been theoretically predicted [9–11] to attain the properties of a Chern insulator, a behavior which has been partially confirmed by ultrafast electronic pump-probe measurements [12,13]. The manipulation of other Floquet topological phases [14–25] and the engineering of topological bands [26–38] have also been proposed. For example, using a gradient-free optimization technique, Zhang and Gong [39] demonstrated the optimization of the Chern numbers of a continuously driven Harper model.

Thus far, however, this field has fallen short on two important points: (i) In order to create a material with a given property, one should not only ensure that the Floquet bands have a particular shape, but also ensure that the electrons occupy the relevant bands. For example, the topological character, classified by the Chern number, is given by the integrated Berry curvature of the bands, which depends on
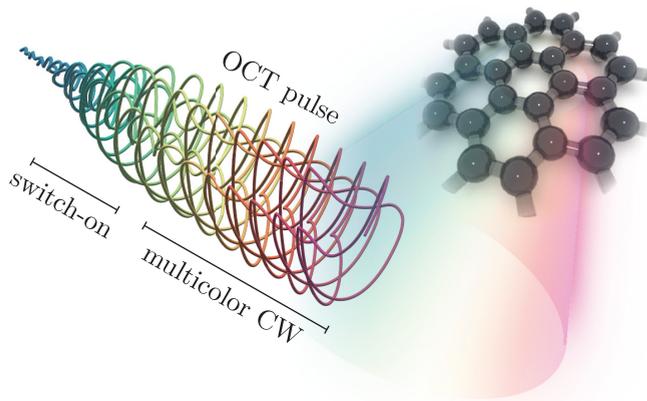
FIG. 1. Schematic diagram of the technique demonstrated in this paper: A graphene sheet is first pumped by a switch-on pulse, that is designed by OCT techniques to prepare the system such that the Floquet bands induced by a periodic multicolor continuous-wave (CW) pulse, that comes later, are populated. This time-periodic driving is also designed by OCT methods, in order to produce Floquet bands with a given predefined shape.

the occupations of the states. (ii) The touted promise of band engineering has been limited to creating replica bands with hybridization gaps [1,2], instead of designing or largely modifying band structures in a stricter sense.

In this paper we address these two points by demonstrating the design of laser pulses capable of both creating Floquet band structures with predefined dispersion shapes and fully controlling their occupations (see Fig. 1). These two properties, occupation and shape, are in fact controlled by two different pulses. The occupation is determined by how a first pulse connects the equilibrium ground state to the Floquet state, that is to say, by how it is switched on. While some works take note of this fact and simulate the switch-on phase [40] and others have analyzed the role of dissipation in the stabilization of Floquet phases [41–43], most works make strong *a priori* assumptions or approximations of the occupations of Floquet states. We note that a system in a single Floquet state in principle does not absorb energy from the periodic driving laser, which means that it can remain longer in the Floquet state before heating up in the long-time limit. Therefore driving protocols such as the ones discussed here may lead to an enhancement of the prethermal steady-state [44,45] lifetime and thus to the experimental accessibility of Floquet state properties.

While the occupations of the bands are controlled by the initial switch-on pulse, the shape of the Floquet band structure is instead determined by the varying amplitudes and phases of the different frequencies of the continuous driving pulse that comes after the switch-on has been completed. It is important to note that the only condition for the Floquet theorem to apply is that the system Hamiltonian is periodic in time. There is no restriction on the number of frequencies that can be contained in the pulse, beyond the fact that they must be multiples of the fundamental frequency that determines its overall periodicity.

Floquet materials engineering has emerged as a viral field of physics and embodies all studies about how many-body systems can be geared by a periodic drive. Apart from a variety of proposed "well known" Floquet topological structures (such as, for example, Floquet topological insulators and Floquet Weyl semimetals) that replicate existing equilibrium analogs, there is a treasure trove of possible Floquet states which have no equilibrium counterpart. Until now, however, Floquet engineering was limited to opening band gaps and manipulating topological phases with simple drivings. It is to be expected that the use of more complex, multifrequency driving will help to find those more unexpected states. Our work points in that direction, as we will show that both the band shapes and the band occupations can be fully controlled by designing the driving field with optimal control theory.

Specifically, we demonstrate, as a proof of principle, how one can design realistic multicolor driving fields that result in predefined shapes of Floquet bands in parts of the Brillouin zone (BZ), thereby fulfilling the promise of band engineering. One can achieve in this way almost arbitrary band shapes defined as control targets—and, for example, control the effective masses, which can be given a negative, zero, or positive value. We further show that it is possible to design light fields such that a single Floquet band is selectively occupied, thus preparing the system in a single Floquet eigenstate. In this way, one may prepare a steady-state electronic structure that is entirely governed by the properties of that Floquet state. In essence, in the following we provide a practical and efficient theoretical framework to design at will the electronic band structure of a material, by designing a multifrequency periodic pumping. The approach relies on merging electronic structure and quantum optical control theory methods in a seamless way.

Finally, we note that by shaping the band structure, one is effectively shaping the nature of electron correlations (e.g., flat bands are connected in many cases to strong electron correlation effects and other rich phenomena). It is an intriguing possibility to study the manipulation of laser-induced electronic correlations with optimal control, which we, however, leave for future work.

In Sec. II we present the graphene model that we have used, with and without the presence of time-dependent periodic perturbations, that can then be described with the help of Floquet formalism. Section III presents the combination of optimal control theory and the Floquet formalism that we propose in order to perform Floquet engineering of the materials. Section IV shows results for some band engineering possibilities: band flattening, band curvature inversion, and gap closing. Finally, Sec. V summarizes our conclusions.

II. MODEL

In the following we will first briefly describe the tight-binding model of graphene that we have used and its behavior under circularly polarized laser pumping, using Floquet theory. This will serve as the reference system for this proof-of-principle work.

We demonstrate the practical feasibility of true Floquet band engineering using graphene as an example, because it has been widely discussed in this context. We use this simple model of independent electrons that describes the low-energy

states of graphene [46,47]:

$$H_{\mathbf{k}} = -\tau \begin{pmatrix} 0 & \Delta(\mathbf{k}) \\ \Delta^*(\mathbf{k}) & 0 \end{pmatrix}, \tag{1}$$

where

$$\Delta(\mathbf{k}) = e^{-ik_x a}\left[1 + 2e^{i3k_x a/2}\cos\left(\frac{\sqrt{3}}{2}k_y a\right)\right], \tag{2}$$

with $a = 2.68$ a.u. being the lattice constant, and $\tau = 0.127$ a.u. This model parametrizes the π bands of graphene, containing the linear dispersing Dirac regions around the K points of the Brillouin zone. Upon irradiation with an electric field (to be treated in what follows in the long-wavelength or dipole approximation), this Hamiltonian must be modified to include an applied time-dependent vector potential $\mathbf{A}(t)$; this can be achieved with the substitution $\mathbf{k} \to \mathbf{k} + \mathbf{A}(t)$.

For a vector potential with periodicity $T = 2\pi/\Omega$, Floquet theory can be applied. We start by defining the Floquet bands $\epsilon_{\mathbf{k}\alpha}$ (also known as pseudoenergies, or pseudobands) in terms of the eigenvalues of the evolution operator at the periodic time T:

$$U_{\mathbf{k}}(T)\big|u_{\mathbf{k}}^\alpha\big\rangle = e^{-i\epsilon_{\mathbf{k}\alpha}T}\big|u_{\mathbf{k}}^\alpha\big\rangle. \tag{3}$$

Because, in our case, the basis space of the model is two dimensional, there are only two eigenvalues per k point ($\alpha = 0, 1$). However, note that the pseudobands are only defined modulo Ω, such that all $\epsilon_{\mathbf{k}\alpha}^{(n)} = \epsilon_{\mathbf{k}\alpha} + n\Omega$ (for all $n \in \mathbb{Z}$) are valid values. These replicas of the pseudobands are often called sidebands. One may also define a so-called "effective" Hamiltonian that verifies

$$U_{\mathbf{k}}(T) = e^{-iH_{\mathbf{k}}^{\mathrm{eff}}T}. \tag{4}$$

It must have the same eigenstates, $H_{\mathbf{k}}^{\mathrm{eff}}|u_{\mathbf{k}}^\alpha\rangle = \epsilon_{\mathbf{k}\alpha}|u_{\mathbf{k}}^\alpha\rangle$, also called the Floquet modes. These can be used to expand any solution to Schrödinger's equation as

$$|\psi_{\mathbf{k}}(t)\rangle = \sum_\alpha f_{\mathbf{k}\alpha}e^{i\epsilon_{\mathbf{k}\alpha}t}\big|u_{\mathbf{k}}^\alpha(t)\big\rangle. \tag{5}$$

In this equation, the time-dependent Floquet modes $|u_{\mathbf{k}}^\alpha(t)\rangle$ are defined from the following propagation of the static modes $|u_{\mathbf{k}}^\alpha\rangle$ [which were defined through Eq. (3)]:

$$\big|u_{\mathbf{k}}^\alpha(t)\big\rangle = e^{-i\epsilon_{\mathbf{k}\alpha}t}U_{\mathbf{k}}(t)\big|u_{\mathbf{k}}^\alpha\big\rangle. \tag{6}$$

These modes are time periodic. The complex coefficients $f_{\mathbf{k}\alpha}$ describe how much each Floquet state is contributing to the dynamics, and hence we define them as the occupation of the Floquet states. Floquet theory permits us to simplify the treatment of periodically driven systems in the following way: Once the evolution of the Floquet modes $|u_{\mathbf{k}}^\alpha(t)\rangle$ in a single period is known (the so-called "micromotion"), the long-term evolution of any state can be easily obtained via Eq. (5).

For practical purposes, it is useful to decompose these time-periodic Floquet modes into their Fourier components,

$$\big|u_{\mathbf{k}}^\alpha(t)\big\rangle = \sum_{m=-\infty}^{\infty}e^{im\Omega t}\big|u_{\mathbf{k}m}^\alpha\big\rangle, \tag{7}$$

$$\big|u_{\mathbf{k}m}^\alpha\big\rangle = \frac{1}{T}\int_0^T dt\, e^{-im\Omega t}|u_{\mathbf{k}\alpha}(t)\rangle, \tag{8}$$

which can then be found using the following eigenvalue equation (which must be truncated at some finite harmonic component value):

$$\sum_n \mathcal{H}_{\mathbf{k}}^{mn}\big|u_{\mathbf{k}n}^\alpha\big\rangle = \epsilon_{\alpha\mathbf{k}}\big|u_{\mathbf{k}m}^\alpha\big\rangle, \tag{9}$$

$$\mathcal{H}_{\mathbf{k}}^{mn} = \frac{\Omega}{2\pi}\int_{2\pi/\Omega}dt\, e^{i(m-n)\Omega t}H_{\mathbf{k}}(t) + \delta_{mn}m\Omega, \tag{10}$$

where m and n label the harmonic components of each Floquet eigenstate and α labels the pseudoband. These Fourier modes, which can be identified with the sidebands mentioned above, correspond to the observed sideband Floquet states in ARPES experiments.

The recently most widely discussed [12,48–52] case of Floquet engineering is the possibility of endowing a material with topological properties by applying circularly polarized light, in particular, in the case of graphene. Figure 2(a) shows the Floquet bands at the Dirac point of graphene under circularly polarized illumination with a 6.5 μm wavelength ($\approx$190 meV) and an intensity of 20 MV/m. The linear crossing of the Dirac bands is deformed in the Floquet steady state to admit a band gap (the field-free linearly crossing bands are also shown for reference). The series of replica bands is shown for a cut across the Dirac point in Fig. 2(d). These sidebands are color-coded: The blue intensity is proportional to $|u_{\mathbf{k}m}^\alpha|$, which represents the contribution of the corresponding component in the Fourier expansion to the Floquet state. The states, in their micromotion during a period T, oscillate with different multiple frequencies of the fundamental one, and in this way one can visually see what the relevant frequencies are—which is sometimes referred to as the population of the sidebands. It can be noted that, with increasing harmonic number $|m|$, the contributions become negligibly small.

The characteristic gap opening shown in Fig. 2(a) is, for large frequencies, inversely proportional to the frequency of the applied light and directly proportional to the intensity [9] (although this dependence is only valid in the high-frequency limit). The analysis of the Berry curvature of the Floquet modes (see Fig. 4) shows that they are nonzero and integrate to nontrivial Chern numbers. Defined as the BZ integral of the Berry curvature of all occupied bands, the Chern number is a topological invariant and is connected to the observation of the anomalous quantum Hall effect [46,53,54].

While each of the two Floquet bands of graphene under circularly polarized illumination separately integrates to a Chern number, they have opposite signs: Unless one is completely empty and the other one is completely occupied, the overall system is not in a topological phase. Instead, its steady state would be characterized by a mixture of opposite Chern numbers. Hence the creation of novel Floquet phases requires control over the population of Floquet states. The band engineering with the circularly polarized light in graphene shown in Fig. 2(a) is limited to an opening of a gap at the Dirac point, which may be controlled by the intensity of the light, but this does not address the problem of preparing the system in a state with the appropriate occupations. We will now discuss how optimal control theory (OCT) can be utilized to design pulses that control both the occupations and the shape of the Floquet bands.
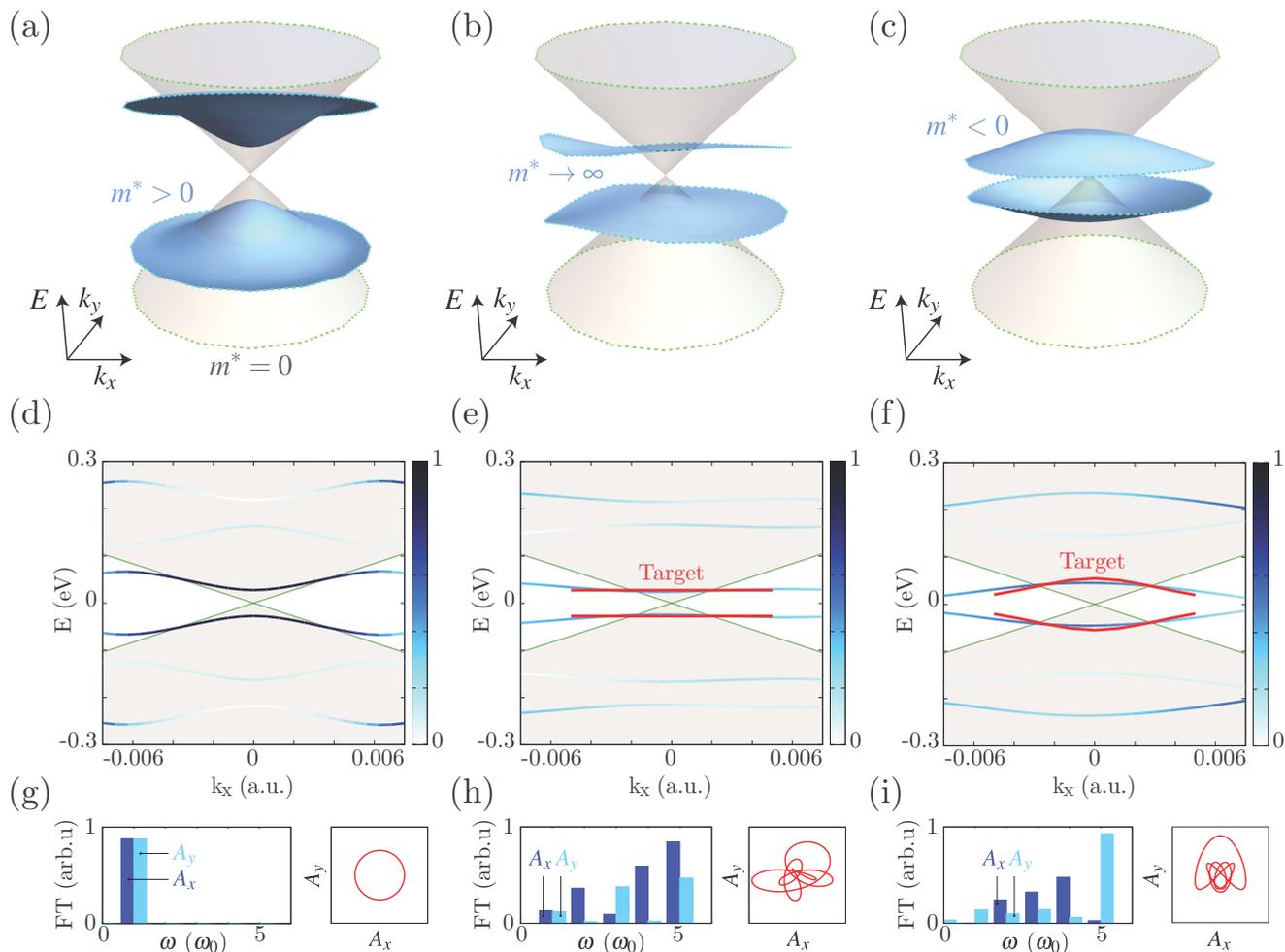
FIG. 2. (a)–(c) Field-free bands (gray) and Floquet pseudobands (blue) of graphene, in the vicinity of the K point. The Floquet pseudobands are computed (a) using a reference circularly polarized field (see text), (b) using fields optimized to create a gap with opposing parallel bands, and (c) using fields optimized to create a gap with opposing concave bands. (d)–(f) Cuts through the xz plane of the previous three-dimensional plots, displaying also the target bands in red and the series of Floquet replicas. These are color-coded: A darker blue color corresponds to a larger Fourier component $\langle u^{\alpha}_{\mathbf{k}m} | u^{\alpha}_{\mathbf{k}m} \rangle$ [see Eqs. (7) and (8)]. (g)–(i) Fourier decomposition (left) and Lissajous plots (right) of the fields corresponding to the pseudobands shown above. FT, Fourier transform.

III. METHOD: QUANTUM OPTIMAL CONTROL THEORY

Optimal control theory addresses the following mathematical problem [55–59]: Given a dynamical system (e.g., Schrödinger's equation) that can be controlled with a set of *control* parameters (e.g., the frequencies and amplitudes of an external electromagnetic field), find those parameters that optimize the behavior of the system with respect to the achievement of some predefined target (e.g., the population of some given state at the end of the process). We are concerned here with two different target definitions: (i) Given a material subject to periodic fields, find the temporal shape of those fields such that the generated Floquet pseudobands most closely resemble some predetermined dispersion, and (ii) given the same material in its ground state, find the shape of the switch-on fields that drive the electrons in a valence band to occupy a given Floquet pseudoband (in particular, the pseudoband induced by the fields that have been optimized previously).

Let us start with a brief description of the method that we have used for target (i). The control parameters $u_1, \ldots, u_P$ will be the Fourier coefficients that determine the shape of the vector potential $\mathbf{A}(t)$:

$$A_x(u, t) = \sum_{n=1}^{M} u_{2n} \cos(\Omega_n t) + u_{2n-1} \sin(\Omega_n t), \quad (11)$$

$$A_y(u, t) = \sum_{n=1}^{M} u_{2M+2n} \cos(\Omega_n t) + u_{2M+2n-1} \sin(\Omega_n t). \quad (12)$$

The frequencies $\Omega_n = \frac{2\pi}{T} n$ are multiples of the fundamental frequency Ω used for the previously described example of graphene irradiated with circularly polarized light, and T is the corresponding period. Note that by using this parametrization we automatically include a *cutoff* frequency $M\Omega$, which also sets the total number of control parameters ($4M$). The existence of a cutoff frequency is a natural experimental

constraint, too. We assume the possibility of independently shaping the fields in the x and y directions.

These fields determine the temporal shape of the Hamiltonian at each $\mathbf{k}$ point: At the low amplitudes that we assume in this paper, we can expand $H_{\mathbf{k}+\mathbf{A}(u,t)}$ in terms of the field $\mathbf{A}(u,t)$ and retain the linear part, i.e.,

$$H_{\mathbf{k}}(u,t) = H_{\mathbf{k}} + \sum_{i=x,y} A_i(u,t) H_{\mathbf{k}}^i. \qquad (13)$$

These Hamiltonians, in turn, determine the evolution operators:

$$i \frac{\partial U_{\mathbf{k}}[u]}{\partial t}(t) = H_{\mathbf{k}}(u,t) U_{\mathbf{k}}[u](t), \qquad (14)$$

$$U_{\mathbf{k}}[u](0) = I. \qquad (15)$$

The Floquet pseudobands $\epsilon_{\mathbf{k}\alpha}(u)$ and the corresponding Floquet modes $|u_{\mathbf{k}}^{\alpha}(u)\rangle$ can then be defined using the eigenvalues and eigenfunctions of the evolution operator at the periodic time T:

$$U_{\mathbf{k}}[u](T) = \sum_{\alpha} e^{-i\epsilon_{\mathbf{k}\alpha}(u)T} |u_{\mathbf{k}}^{\alpha}(u)\rangle\langle u_{\mathbf{k}}^{\alpha}(u)|. \qquad (16)$$

Suppose now that we wish for the external fields to induce a given set of pseudobands $\tilde{\epsilon}_{\mathbf{k}\alpha}$ and Floquet modes $|\tilde{u}_{\mathbf{k}}^{\alpha}\rangle$. This would be equivalent to asking the perturbation fields to induce an evolution operator given by

$$\tilde{U}_{\mathbf{k}} = \sum_{\alpha} e^{-i\tilde{\epsilon}_{\mathbf{k}\alpha}T} |\tilde{u}_{\mathbf{k}}^{\alpha}\rangle\langle \tilde{u}_{\mathbf{k}}^{\alpha}|. \qquad (17)$$

One can use quantum optimal control theory for the generation of target evolution operators. This concept was first developed for the problem of designing quantum gates within quantum information theory studies [60]. However, we may use it for the problem at hand—with the added complication that the target must be simultaneously formulated for a set of $\mathbf{k}$ points.

Thus the mathematical formulation of the optimization problem can be established by defining the following target functional:

$$F(U_{\mathbf{k}}[u](T)) = \frac{1}{N_{\mathrm{kps}}} \sum_{\mathbf{k} \in \mathcal{K}} |\tilde{U}_{\mathbf{k}} \cdot U_{\mathbf{k}}[u](T)|^2, \qquad (18)$$

where we use the Frobenius dot product for operators,

$$A \cdot B = \frac{1}{d} \mathrm{Tr} A^{\dagger} B. \qquad (19)$$

d is the dimension of the operators, which in our case is 2. N_{kps} is the number of $\mathbf{k}$ points in the set $\mathcal{K}$: This is a finite set of points in the Brillouin zone that defines the region of interest. The goal is to engineer the band structure in this region. Here, we will work with a disk-shaped region defined around the K point of graphene.

The functional in Eq. (18) takes a maximum value equal to 1 when the generated evolution operators $U_{\mathbf{k}}[u](T)$ are equal to the target ones $\tilde{U}_{\mathbf{k}}$ (or are equivalent, i.e., related by a global multiplicative phase factor). The goal is therefore finding the parameters u that lead to those evolutions: The problem finally boils down to the maximization of the function:

$$G(u) = F(U_{\mathbf{k}}[u](T)). \qquad (20)$$

Note that, in this paper, we are only interested in the shape of the pseudobands $\epsilon_{\mathbf{k}\alpha}$, regardless of the modes $|u_{\mathbf{k}}^{\alpha}\rangle$. However, in the formulation described above, we need to specify the target modes $|\tilde{u}_{\mathbf{k}}^{\alpha}\rangle$. In this paper, we have simply set those modes to be equal to the field-free states associated with the corresponding band [61].

In order to find the maximum of a multivariate function G, there is a plethora of available algorithms; the most efficient ones require the use of the gradient $\nabla G(u)$. We have used the sequential least-squares quadratic programming (SLSQP) algorithm [62] as implemented in the NLOPT library [63]. Optimal control theory permits us to derive an expression for the gradient (essentially, as an application of Pontryagin's maximum principle [64]),

$$\frac{\partial G}{\partial u_m}(u) = \frac{1}{N_{\mathrm{kps}}} \sum_{i=x,y} \sum_{\mathbf{k} \in \mathcal{K}} 2\,\mathrm{Im} \int_0^{t_f} dt \, \frac{\partial A_i}{\partial u_m}(u,t)$$
$$\times B_{\mathbf{k}}[u](t) \cdot \left(H_{\mathbf{k}}^i(t) U_{\mathbf{k}}[u](t) \right), \qquad (21)$$

where the *costate* $B_{\mathbf{k}}[u](t)$ is defined by the following equations:

$$i \frac{\partial}{\partial t} B_{\mathbf{k}}[u](t) = H_{\mathbf{k}}(u,t) B_{\mathbf{k}}[u](t), \qquad (22)$$

$$B_{\mathbf{k}}[u](T) = (\tilde{U}_{\mathbf{k}} \cdot U_{\mathbf{k}}[u](T)) \tilde{U}_{\mathbf{k}}. \qquad (23)$$

This equation of motion is analogous to the one that defines the evolution operator $U_{\mathbf{k}}[u](t)$, except for the boundary condition, which is given at the final time of the propagation T: It is a *final* condition, instead of an initial condition.

Note that the parameter search space is not unbounded, as that would allow for solution fields with arbitrary intensities, which would be experimentally impractical. We imposed bound constraints, $|u_m| \leqslant \kappa$, for some predefined bound κ.

Equations (21)–(23) enable us to compute the gradient of the function G defined in Eq. (20), which allows its maximization, and the solution of the first OCT problem mentioned above: (i) finding the periodic drivings that permit the Floquet pseudoband engineering. The second OCT problem—(ii) finding the switch-on laser pulses that permit us to populate those pseudobands starting from the material at equilibrium—is a more conventional one. In this case, the problem and the target functional are not defined in terms of the evolution operator of the system, but rather in terms of the material states. The goal is to drive the electrons in the valence band towards the Floquet modes; the states are driven by Schrödinger's equation in the presence of a switch-on time-dependent Hamiltonian:

$$i \frac{\partial \psi_{\mathbf{k}\alpha}[v]}{\partial t}(t) = H_{\mathbf{k}}(v,t) \psi_{\mathbf{k}\alpha}[v](t), \qquad (24)$$

$$\psi_{\mathbf{k}\alpha}[v](0) = \psi_{\mathbf{k}\alpha}, \qquad (25)$$

where α is the valence band index ($\alpha = 0$, in our case). The switch-on pulses are given by two vector field functions $A_x^{\mathrm{so}}(v,t)$ and $A_y^{\mathrm{so}}(v,t)$ that operate for a time T_{so}, after which they are substituted by the optimal periodic driving that has been found using the method described above. Once again, the shapes of the pulses are determined by a set of parameters v, but in this case the parametrization is different. We have

enforced the following shape:

$$A_i^{so}(v, t) = S(t) f_i(v, t) A_i(u^{opt}, t), \quad i = x, y. \quad (26)$$

Function $S(t) = 3(t/T_{so})^2 - 2(t/T_s)^3$ smoothly varies from zero at $t = 0$ to 1 at $t = T_s$. The fields $A_i(u^{opt}, t)$ are the optimal periodic pulses that induce the target Floquet pseudoband structure. The functions $f_i(v, t)$ are, once again, Fourier series, similar to the ones in Eqs. (11) and (12), and the control parameters v are the corresponding Fourier coefficients. In this case, they are constrained to ensure that $f(v, t = T_{so}) = 1$. With this definition, the periodic pulses $A_i(u^{opt}, t)$ are initiated but are first multiplied by a smooth envelope function $S(t) f_i(v, t)$ that slowly switches from zero to 1 at $t = T_{so}$. After that switch-on pulse time T_{so}, the optimal periodic drivings stay indefinitely. The shape of the optimized envelope should be such that, by the end of the switch-on phase, the ground-state orbitals of the material valence band are transformed into the Floquet modes and, in this way, they are afterwards stationary (in the Floquet sense, that is, *stroboscopically* stationary).

It remains to specify the target functional for this case: If the goal is to maximize the population, at time T_{so}, of the Floquet modes $|u_{\mathbf{k}\alpha}\rangle$, the natural choice is

$$F(\psi_{\mathbf{k}\alpha}[v](T_{so})) = \sum_{\mathbf{k} \in \mathcal{K}} |\langle \psi_{\mathbf{k}\alpha}[v](T_{so}) | u_{\mathbf{k}\alpha}\rangle|^2. \quad (27)$$

Function G is now defined in terms of this new functional:

$$G(v) = F(\psi_{\mathbf{k}\alpha}[v](T_{so})), \quad (28)$$

whose gradient is given by [65]

$$\frac{\partial G}{\partial v_m}(v) = \sum_{i=x,y} \sum_{\mathbf{k} \in \mathcal{K}} 2 \, \text{Im} \int_0^{t_f} dt \, \frac{\partial A_i^{so}}{\partial v_m}(v, t)$$
$$\times \langle \chi_{\mathbf{k}\alpha}[v](t) | H_{\mathbf{k}}^i(t) | \psi_{\mathbf{k}\alpha}[v](t)\rangle. \quad (29)$$

The costates $\chi_{\mathbf{k}\alpha}[v](t)$ are now defined by

$$i \frac{\partial}{\partial t} \chi_{\mathbf{k}\alpha}[v](t) = H_{\mathbf{k}}(v, t) \chi_{\mathbf{k}\alpha}[v](t), \quad (30)$$

$$\chi_{\mathbf{k}\alpha}[v](T) = \langle u_{\mathbf{k}\alpha} | \chi_{\mathbf{k}\alpha}[v](T)\rangle u_{\mathbf{k}\alpha}. \quad (31)$$

Equations (29)–(31) permit us to compute the gradient of function G defined in Eq. (28), which can then be fed into any function maximization algorithm to solve the second optimization problem posed above.

Our numerical approach to solving the quantum optimal control theory (QOCT) problem is of course not the only alternative. The general optimal control theory was first applied to quantum systems in the 1980s [66–71], and various algorithms have been proposed over the years [72–74]—one of the most used ones has been Krotov's method [75]. Another very successful option is the gradient ascent pulse engineering (GRAPE) algorithm [76], put forward in the context of control for nuclear magnetic resonance (NMR) applications. A rather common assumption of most of those algorithms, however, is the use of control functions in real time, $u_1(t), \ldots, u_n(t)$, instead of using generic parametrizations of those functions in terms of parameters $u_1, \ldots, u_P$, as we have assumed in the previous equations. We have preferred this option, as in our opinion it facilitates the enforcement of constraints on the

control functions. Note that, in addition to the method that we have described before, some other alternatives designed for the use of arbitrarily parametrized control functions also exist, such as, for example, the so-called gradient optimization of analytic controls (GOAT) [77] and chopped random basis (CRAB) [78] algorithms. The latter, however, is a gradientless algorithm, and the former requires more propagations for the calculation of the gradient. For these reasons we have opted for the described choice—perhaps the method found in the literature that is closest to ours was put forward in Ref. [79].

IV. RESULTS

A. Band engineering

We now describe the obtained results, starting with an optimization of type (i): The first goal was to engineer a periodic driving field that induces Floquet bands that are optimized to resemble two parallel disks in a region around the Dirac point, thus creating a gap in between two flat bands. As the fundamental frequency Ω, we used the same one (corresponding to 6.5 μm) used in the previously discussed reference example with circularly polarized light. We set the cutoff frequency to five times Ω, i.e., $M = 5$ in the parametrization given in Eqs. (11) and (12). Furthermore, we establish a bound constraint for the amplitudes of each individual frequency component ($|u_m| \leqslant \kappa$), where we set κ to match the amplitude of the reference circularly polarized example (20 MV/m).

The radius of the target disks was chosen to be 0.005 a.u., which amounts to $\approx 0.3\%$ of the length of a reciprocal lattice vector. The manipulation of the Floquet bands' shape, in these examples, is therefore limited to a reciprocal space region around the K point of that size. This size was chosen considering that we are interested in some energy window around the Fermi level: The energy separation of the field-free valence and conduction bands for graphene around the K point (where the Fermi level is placed) at our chosen radius of 0.005 a.u. is already of the order of 0.1 eV [see Fig. 2(c)], and thus, of the order of 1000 K. This is the frequency range that must be used to search for the optimal periodic drivings capable of manipulating the Floquet bands. In the presence of frequencies below those temperatures, the relevant region in reciprocal space is therefore the one that we have used. We note that we have also successfully performed similar optimizations using larger target regions in reciprocal space—at the cost of using a correspondingly larger frequency range for the periodic drivings.

Figure 2(b) shows the resulting bands together with the original Dirac cones. Note that the target region, where the bands are optimized, comprises only a part of the shown area; hence on the edges the disks are slightly bent. Figure 2(e) shows a cut through Fig. 2(b) along the k_x direction, and the target disks are indicated in red. We see here more clearly that the OCT process results in bands that are almost perfectly matching the target in the region where it is defined, and the parallel character of the bands extends somewhat beyond that region.

Parallel bands correspond to states that are well localized in real space, and have been widely discussed in connection with twisted bilayer systems, where the electron localization

is caused by the interaction of the electronic structure at certain twist angles. Here, instead, the driving pulse creates a superposition of valence and conduction states that result in a very similar band structure, but without the need for structural twisting and within the original Brillouin zone. The degree of spatial localization is dictated by how much of the BZ is spanned by the Floquet flat band. In our example in Fig. 2(e) it is around 1%, which is similar to the localization length in moiré materials. Note that this is different from the previously discussed dynamical localization [80], which results from a monochromatic high-frequency drive and which in the case of graphene only results in the bands shown in Fig. 2(b). Instead, the optimized pulse here has a complex frequency structure, as shown in Fig. 2(h): It displays the absolute value of its Fourier components [essentially, the control parameters u; see Eqs. (11) and (12)]. The fundamental frequency for the flat Floquet band optimization is the same as for the simple monochromatic Floquet case in Fig. 2(a), and the gap opens by the same amount; however, the optimized pulse has additional components. Furthermore, it has a nontrivial polarization dynamics, as shown in the right panel of Fig. 2(h), where the Lissajous plot of the electric field is shown [compare with the simple circle in Fig. 2(g)].

Having demonstrated that it is possible to create flat bands in a defined region of the BZ, we take the band engineering one step further to demonstrate that, in principle, arbitrary band shapes can be designed. Figure 2(c) shows a Floquet band structure where the effective mass of the bands has been inverted relative to the monochromatic case: Instead of a convex band with a positive effective mass, it is possible to create a concave band where the effective mass is negative. Figure 2(f) is a cut along Fig. 2(c), and it shows in red the target bands, along with the Floquet bands and sidebands, in varying tones of blue, once again graded according to their Fourier component magnitude. While for the present case there is no direct application of such band inversion (at least to our knowledge), in other materials it will result in drastically altered optical properties.

For completeness, we have also attempted an optimization with the target of closing a gap, rather than opening it as in the previous cases. Since graphene does not have a gap, we have modified the graphene model that we have used, adding to the static Hamiltonian the term

$$H_{\mathbf{k}}^{\text{gap}} = \begin{pmatrix} \delta/2 & 0 \\ 0 & -\delta/2 \end{pmatrix}, \tag{32}$$

which creates a gap in the K point. This modification corresponds to the trivial part of the Haldane model [46]. We have not used the off-diagonal terms of the Haldane model, which determine its topological properties, since those would not change the discussion below about closing the band gap. For the value of the gap δ we have chosen 0.01 a.u. $\approx$ 270 meV. The modified field-free bands of this model are shown in Fig. 3(a), in gray [and also in Fig. 3(b), which is a cut of Fig. 3(a) along direction y]. We have then performed an optimization with the target of closing the gap at point K: For that purpose, we used the functional defined in Eq. (18), using only the K point to define the set $\mathcal{K}$ and setting the target pseudoenergies of both bands to zero. The resulting optimal pseudobands are shown in both Figs. 3(a) and 3(b): It can
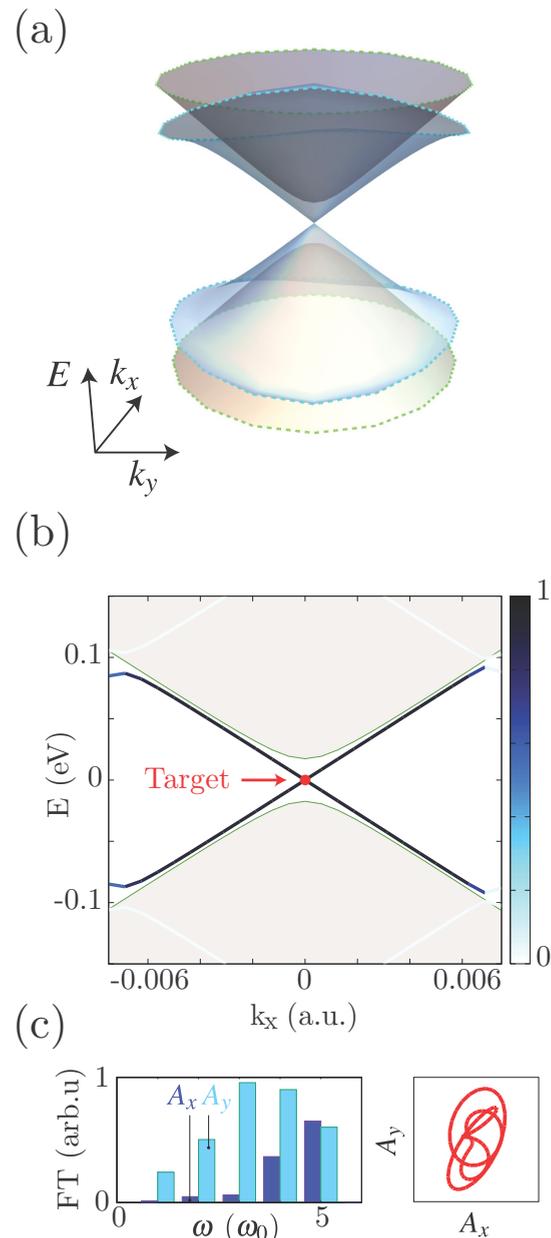
FIG. 3. Gap closing. (a) Field-free bands (gray) of the modified graphene model in the vicinity of the K point (blue) showing how the gap can be closed. (b) Cut along the y axis of (a). Along with the Floquet bands in the first BZ, the sidebands are also shown. The color intensity of each point is proportional to the value of the corresponding Fourier component. (c) Fourier components and Lissajous figure of the optimized pulse.

be seen how the optimization is successful and the gap is effectively closed.

We now discuss how the flexible band engineering by OCT shown above is accompanied by changes to the Berry curvature. In this paper, we chose not to design pulses that target specific Berry curvatures or topologies, although this is in principle possible. However, for completeness, we show in Fig. 4 the Berry curvature for the Floquet pseudobands obtained with the optimal pulses shown above (and also with the
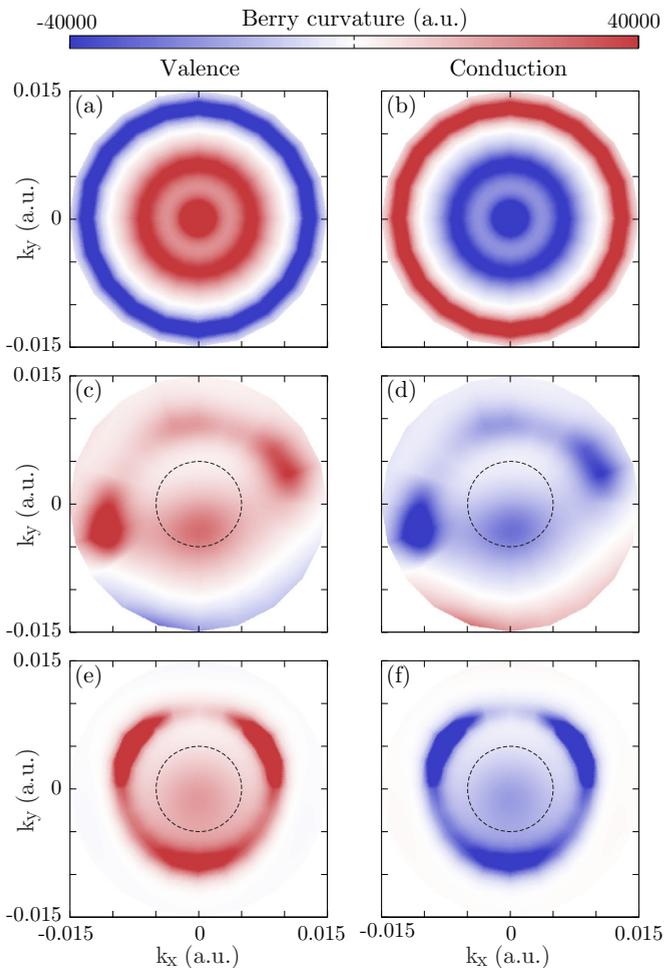
FIG. 4. Berry curvature of the valence (left panels) and conduction (right panels) pseudobands. They correspond to (a) and (b) the Floquet pseudobands computed with the reference circularly polarized fields, (c) and (d) the flat pseudobands, and (e) and (f) the negative curvature bands shown in Fig. 2. (a) replicates the results shown in Fig. 3(d) of Ref. [13]. Black dashed circles indicate the area for which the target was defined.

reference monochromatic circularly polarized fields), computed as

$$\Omega_{\mathrm{B}}(\mathbf{k}) = \frac{-i}{T} \int_0^T dt \left[\nabla_{\mathbf{k}} \times \left\langle u_{\mathbf{k}}^\alpha(t) \middle| \nabla_{\mathbf{k}} \middle| u_{\mathbf{k}}^\alpha(t) \right\rangle \right]_z. \tag{33}$$

Here, $\alpha = 0, 1$ for the lower (valence) and higher (conduction) pseudoenergy Floquet pseudoband, respectively. We display them separately in the left [Figs. 4(a), 4(c), and 4(e)] and right [Figs. 4(b), 4(d), and 4(f)] panels of Fig. 4. It can be seen that, while the Berry curvature of the Floquet states obtained with the monochromatic circular pulse varies strongly, the curvatures of the pseudobands obtained with the two optimized cases show more gradual changes. It can also be seen how valence and conduction curvatures take approximately inverse values. We note that a region of the BZ outside the target area is also shown; inside the target area the Berry curvature is very small in both cases. The variations seem to be the result of small changes in the optimal results. This indicates the sensitivity of the Berry curvature to the shape
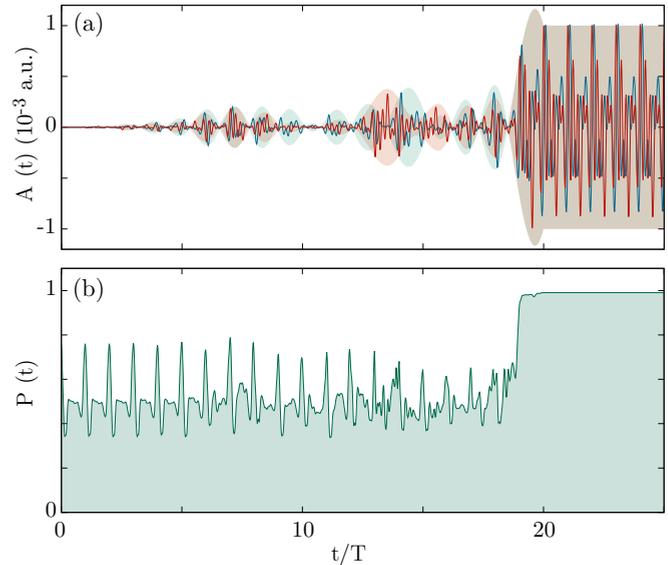
FIG. 5. (a) Optimal switch-on A_x^{so} (blue) and A_y^{so} (red) pulses, applied during the first 20 periods of duration T, followed by the optimized periodic drivings A_x and A_y. Lines represent the full pulses $A_i^{\mathrm{so}}(v^{\mathrm{opt}}, t) = S(t) f_i(v^{\mathrm{opt}}, t) A_i(u^{\mathrm{opt}}, t)$, whereas the filled curves are the absolute value of the envelopes $S(t) f_i(v^{\mathrm{opt}}, t)$ (which become equal to 1 after the switch-on phase). (b) Average population of the lower pseudoenergy Floquet modes: $|\langle \psi_{\mathbf{k}0}(t) | u_{\mathbf{k}}^0(t) \rangle|^2$. One can see how, after the switch-on phase, it is approximately constant and equal to 1 since the system has been (almost) transferred to those states.

of the bands and to the driving protocol. This would hint that an optimization protocol that would directly target the Berry curvature could be very efficient in manipulating this property. This would entail a target definition not only in terms of the bands, but also in terms of the modes. In the calculations presented here, the target bands were arbitrarily set to match the field-free eigenstates, at least at the stroboscopic times 0, T, $2T$, etc. The optimal modes obtained are therefore similar, but not equal, to those states.

B. Design of the switch-on pulse

For the Floquet engineering of materials to be practically useful, one also needs to be in full control of the occupation of bands: The material properties depend not only on the band shapes, but also on how they are occupied. Therefore, before the periodic drivings are started, there should be a switch-on phase in which a pulse leads the electrons in the valence bands to occupy the Floquet bands of interest. OCT can be used to design this switch-on pulse, and we show in Fig. 5 one example, demonstrating that it is possible to target the full occupation of a single Floquet state. In particular, this plot corresponds to the problem of the design of flat bands. The target is to transfer the electrons in the equilibrium valence band to the lower Floquet pseudoband that was found via the previous optimization process (in the target region defined previously, a disk around the K point of the BZ).

As discussed in the previous section, we have enforced some constraints on the switch-on pulse, since we are aware that the experimental realization of these ideas would also

face technical constraints. For this proof-of-principle study, we have envisioned a switch-on phase that consists of the same periodic drives that are later responsible for the tailored bands, but multiplied by a smooth envelope that slowly ramps from zero to 1. This envelope admits some low frequencies, and the amplitudes of these are the control parameters in the optimization process. One also needs to specify a duration for the switch-on phase; in our case we have set it to 20 times the fundamental period of the periodic drive $T \approx 21.7$ fs. Figure 5(a) displays the resulting optimal pulses; the thin lines are the full electric fields [Eq. (26)], whereas the shaded filled curves are the envelopes. One can see how they smoothly morph into the periodic drives. Of course, the true experimental constraints regarding the maximal frequencies or amplitudes may vary, but the OCT methodology that we have described may be adapted accordingly.

To illustrate the evolution of the Floquet occupations under the optimized pulses, we show the average of the square modules of the projection of the time-evolving states onto the Floquet states $|u_{\mathbf{k}}^0(t)\rangle$ ("0" is the index of the lower pseudoband):

$$P(t) = \frac{1}{N_{\text{kps}}} \sum_{k \in \mathcal{K}} |\langle \psi_{\mathbf{k}0}(t)|u_{\mathbf{k}}^0(t)\rangle|^2. \qquad (34)$$

By design, the switch-on pulse stops once the occupation has reached unity, after which the periodic Floquet driving is activated and the occupation remains (approximately) constant, as intended.

V. CONCLUSIONS

We have demonstrated, by performing proof-of-principle OCT calculations, that one can create and control the nonequilibrium steady-state Floquet phase with an unprecedented range of versatility, by finding the necessary multifrequency periodic drivings. The Floquet band structure of materials can thus be shaped at will over the regions of the Brillouin zone deemed to be relevant in each case. This has strong implications for optical and transport properties. We have not used global or local topological properties as optimization targets, but the sensitivity of the Berry curvature shown here clearly indicates that manipulation of this and other topological properties is possible. Thus this proposed design of driving pulses is an important step towards designing quantum materials "on demand" [81].

We have exemplified our proposal inspired by the experiment reported by McIver *et al.* [12], who measured a light-induced anomalous Hall effect in monolayer graphene,

driven by a femtosecond pulse of circularly polarized light. The model that we have used permits us to describe such an experiment [13]. The driving field parameters (intensity, frequency) of our model are of the same order as the experimental parameters [12]. Therefore the only ingredient missing to implement the control scheme described here would be the ability to shape the perturbations as a combination of five frequencies, rather than using a simple monochromatic one. However, laser shaping technologies have fast advanced in the last decades.

Furthermore, we have not only optimized the Floquet band structure shape by designing the periodic drivings, but also demonstrated the possibility of controlling the occupation of Floquet states via a switch-on pulse optimization. Here, we have assumed a closed quantum system and employed a single-electron tight-binding model. However, the case of correlated materials can be treated similarly and is left for a future work. The results shown in this paper are naturally transportable to the case of including electron correlations in the Hamiltonian.

Finally, the discussed scheme also offers a route towards controlling the stability of Floquet states and affecting their long-time behavior. It is expected that in the early times a system will absorb significantly less energy when prepared as a single Floquet eigenstate, because the entire dressed state, electronic structure and laser, is an eigenstate of the time-dependent Schrödinger equation. However, decoherence, dissipation effects, and scattering pathways that are not included in the Schrödinger equation can affect this state. Therefore the state will eventually lose its pure Floquet character and gradually heat up to $T \to \infty$ at infinite times. However, the so-called Floquet prethermal state may last much longer for a pure Floquet state, thus making it accessible for technological applications. Additionally, one could envision OCT schemes that account for the major decoherence channels and thereby design pulses that counteract them, and thus one could increase the Floquet states' lifetimes. The extension of the current work to deal with these issues by considering open quantum systems is a work in progress.

[1] Y. H. Wang, H. Steinberg, P. Jarillo-Herrero, and N. Gedik, Observation of Floquet-Bloch states on the surface of a topological insulator, Science **342**, 453 (2013).

[2] F. Mahmood, C.-K. Chan, Z. Alpichshev, D. Gardner, Y. Lee, P. A. Lee, and N. Gedik, Selective scattering between Floquet-Bloch and Volkov states in a topological insulator, Nat. Phys. **12**, 306 (2016).

[3] S. Aeschlimann, S. A. Sato, R. Krause, M. Chávez-Cervantes, U. de Giovannini, H. Hübener, S. Forti, C. Coletti, K. Hanff, K. Rossnagel, A. Rubio, and I. Gierz, Survival of Floquet–Bloch states in the presence of scattering, Nano Lett. **21**, 5028 (2021).

[4] B. M. Fregoso, Y. H. Wang, N. Gedik, and V. Galitski, Driven electronic states at the surface of a topological insulator, Phys. Rev. B **88**, 155129 (2013).

[5] M. A. Sentef, M. Claassen, A. F. Kemper, B. Moritz, T. Oka, J. K. Freericks, and T. P. Devereaux, Theory of Floquet band formation and local pseudospin textures in pump-probe photoemission of graphene, Nat. Commun. **6**, 7047 (2015).

[6] U. De Giovannini, H. Hübener, and A. Rubio, Monitoring electron-photon dressing in WSe$_2$, Nano Lett. **16**, 7993 (2016).

[7] U. D. Giovannini and H. Hübener, Floquet analysis of excitations in materials, J. Phys.: Mater. **3**, 012001 (2020).

[8] U. De Giovannini, S. A. Sato, H. Hübener, and A. Rubio, First-principles modelling for time-resolved ARPES under different pump–probe conditions, J. Electron Spectrosc. Relat. Phenom. **254**, 147152 (2022).

[9] T. Oka and H. Aoki, Photovoltaic Hall effect in graphene, Phys. Rev. B **79**, 081406(R) (2009).

[10] T. Kitagawa, E. Berg, M. Rudner, and E. Demler, Topological characterization of periodically driven quantum systems, Phys. Rev. B **82**, 235114 (2010).

[11] J.-i. Inoue and A. Tanaka, Photoinduced Transition between Conventional and Topological Insulators in Two-Dimensional Electronic Systems, Phys. Rev. Lett. **105**, 017401 (2010).

[12] J. W. McIver, B. Schulte, F.-U. Stein, T. Matsuyama, G. Jotzu, G. Meier, and A. Cavalleri, Light-induced anomalous Hall effect in graphene, Nat. Phys. **16**, 38 (2020).

[13] S. A. Sato, J. W. McIver, M. Nuske, P. Tang, G. Jotzu, B. Schulte, H. Hübener, U. De Giovannini, L. Mathey, M. A. Sentef, A. Cavalleri, and A. Rubio, Microscopic theory for the light-induced anomalous Hall effect in graphene, Phys. Rev. B **99**, 214302 (2019).

[14] R. Wang, B. Wang, R. Shen, L. Sheng, and D. Y. Xing, Floquet Weyl semimetal induced by off-resonant light, Europhys. Lett. **105**, 17004 (2014).

[15] C.-K. Chan, Y.-T. Oh, J. H. Han, and P. A. Lee, Type-II Weyl cone transitions in driven semimetals, Phys. Rev. B **94**, 121106(R) (2016).

[16] C.-K. Chan, P. A. Lee, K. S. Burch, J. H. Han, and Y. Ran, When Chiral Photons Meet Chiral Fermions: Photoinduced Anomalous Hall Effects in Weyl Semimetals, Phys. Rev. Lett. **116**, 026805 (2016).

[17] S. Ebihara, K. Fukushima, and T. Oka, Chiral pumping effect induced by rotating electric fields, Phys. Rev. B **93**, 155107 (2016).

[18] Z. Yan and Z. Wang, Tunable Weyl Points in Periodically Driven Nodal Line Semimetals, Phys. Rev. Lett. **117**, 087402 (2016).

[19] A. Narayan, Tunable point nodes from line-node semimetals via application of light, Phys. Rev. B **94**, 041409(R) (2016).

[20] H. Hübener, M. A. Sentef, U. De Giovannini, A. F. Kemper, and A. Rubio, Creating stable Floquet-Weyl semimetals by laser-driving of 3D Dirac materials, Nat. Commun. **8**, 13940 (2017).

[21] Z. Yan and Z. Wang, Floquet multi-Weyl points in crossing-nodal-line semimetals, Phys. Rev. B **96**, 041206(R) (2017).

[22] M. Ezawa, Photoinduced topological phase transition from a crossing-line nodal semimetal to a multiple-Weyl semimetal, Phys. Rev. B **96**, 041205(R) (2017).

[23] Z. F. Wang, Z. Liu, J. Yang, and F. Liu, Light-Induced Type-II Band Inversion and Quantum Anomalous Hall State in Monolayer FeSe, Phys. Rev. Lett. **120**, 156406 (2018).

[24] C. P. Weber, Ultrafast investigation and control of Dirac and Weyl semimetals, J. Appl. Phys. **129**, 070901 (2021).

[25] P. Titum, E. Berg, M. S. Rudner, G. Refael, and N. H. Lindner, Anomalous Floquet-Anderson Insulator as a Nonadiabatic Quantized Charge Pump, Phys. Rev. X **6**, 021013 (2016).

[26] N. H. Lindner, G. Refael, and V. Galitski, Floquet topological insulator in semiconductor quantum wells, Nat. Phys. **7**, 490 (2011).

[27] M. Ezawa, Photoinduced Topological Phase Transition and a Single Dirac-Cone State in Silicene, Phys. Rev. Lett. **110**, 026603 (2013).

[28] Y. T. Katan and D. Podolsky, Modulated Floquet Topological Insulators, Phys. Rev. Lett. **110**, 016802 (2013).

[29] A. Narayan, Floquet dynamics in two-dimensional semi-Dirac semimetals and three-dimensional Dirac semimetals, Phys. Rev. B **91**, 205445 (2015).

[30] M. Claassen, C. Jia, B. Moritz, and T. P. Devereaux, All-optical materials design of chiral edge modes in transition-metal dichalcogenides, Nat. Commun. **7**, 13074 (2016).

[31] L. D'Alessio and M. Rigol, Dynamical preparation of Floquet Chern insulators, Nat. Commun. **6**, 8336 (2015).

[32] C. Dutreix, E. A. Stepanov, and M. I. Katsnelson, Laser-induced topological transitions in phosphorene with inversion symmetry, Phys. Rev. B **93**, 241404(R) (2016).

[33] H. Wang, L. Zhou, and Y. D. Chong, Floquet Weyl phases in a three-dimensional network model, Phys. Rev. B **93**, 144114 (2016).

[34] X.-X. Zhang, T. T. Ong, and N. Nagaosa, Theory of photoinduced Floquet Weyl semimetal phases, Phys. Rev. B **94**, 235137 (2016).

[35] R. Roy and F. Harper, Periodic table for Floquet topological insulators, Phys. Rev. B **96**, 155118 (2017).

[36] H. Liu, J.-T. Sun, C. Cheng, F. Liu, and S. Meng, Photoinduced Nonequilibrium Topological States in Strained Black Phosphorus, Phys. Rev. Lett. **120**, 237403 (2018).

[37] P. X. Nguyen and W.-K. Tse, Photoinduced anomalous Hall effect in two-dimensional transition metal dichalcogenides, Phys. Rev. B **103**, 125420 (2021).

[38] L. Zhou and J. Gong, Recipe for creating an arbitrary number of Floquet chiral edge states, Phys. Rev. B **97**, 245430 (2018).

[39] S. Zhang and J. Gong, Floquet engineering with particle swarm optimization: Maximizing topological invariants, Phys. Rev. B **100**, 235452 (2019).

[40] M. H. Kalthoff, G. S. Uhrig, and J. K. Freericks, Emergence of Floquet behavior for lattice fermions driven by light pulses, Phys. Rev. B **98**, 035138 (2018).

[41] H. Dehghani, T. Oka, and A. Mitra, Dissipative Floquet topological systems, Phys. Rev. B **90**, 195429 (2014).

[42] H. Dehghani, T. Oka, and A. Mitra, Out-of-equilibrium electrons and the Hall conductance of a Floquet topological insulator, Phys. Rev. B **91**, 155422 (2015).

[43] K. I. Seetharam, C.-E. Bardyn, N. H. Lindner, M. S. Rudner, and G. Refael, Controlled Population of Floquet-Bloch States via Coupling to Bose and Fermi Baths, Phys. Rev. X **5**, 041050 (2015).

[44] S. A. Weidinger and M. Knap, Floquet prethermalization and regimes of heating in a periodically driven, interacting quantum system, Sci. Rep. **7**, 45382 (2017).

[45] A. Haldar, R. Moessner, and A. Das, Onset of Floquet thermalization, Phys. Rev. B **97**, 245122 (2018).

[46] F. D. M. Haldane, Model for a Quantum Hall Effect without Landau Levels: Condensed-Matter Realization of the "Parity Anomaly", Phys. Rev. Lett. **61**, 2015 (1988).

[47] A. H. Castro Neto, F. Guinea, N. M. R. Peres, K. S. Novoselov, and A. K. Geim, The electronic properties of graphene, Rev. Mod. Phys. **81**, 109 (2009).

[48] G. Jotzu, M. Messer, R. Desbuquois, M. Lebrat, T. Uehlinger, D. Greif, and T. Esslinger, Experimental realization of the topological Haldane model with ultracold fermions, Nature (London) **515**, 237 (2014).

[49] A. A. Burkov, M. D. Hook, and L. Balents, Topological nodal semimetals, Phys. Rev. B **84**, 235126 (2011).

[50] T. Oka and S. Kitamura, Floquet engineering of quantum materials, Annu. Rev. Condens. Matter Phys. **10**, 387 (2019).

[51] M. S. Rudner and N. H. Lindner, Band structure engineering and non-equilibrium dynamics in Floquet topological insulators, Nat. Rev. Phys. **2**, 229 (2020).

[52] C. Bao, P. Tang, D. Sun, and S. Zhou, Light-induced emergent phenomena in 2D materials and topological materials, Nat. Rev. Phys. **4**, 33 (2022).

[53] C. L. Kane and E. J. Mele, Z_2 Topological Order and the Quantum Spin Hall Effect, Phys. Rev. Lett. **95**, 146802 (2005).

[54] C.-Z. Chang, Z. Jinsong, F. Xiao, S. Jie, Z. Zuocheng, G. Minghua, L. Kang, O. Yunbo, W. Pang, W. Li-Li, J. Zhong-Qing, F. Yang, J. Shuaihua, C. Xi, J. Jinfeng, D. Xi, F. Zhong, Z. Shou-Cheng, H. Ke, W. Yayu *et al.*, Experimental observation of the quantum anomalous Hall effect in a magnetic topological insulator, Science **340**, 167 (2013).

[55] D. E. Kirk, *Optimal Control Theory. An Introduction* (Dover, New York, 1998).

[56] P. Brumer and M. Shapiro, *Principles of the Quantum Control of Molecular Processes* (Wiley, New York, 2003).

[57] C. Brif, R. Chakrabarti, and H. Rabitz, Control of quantum phenomena: Past present and future, New J. Phys. **12**, 075008 (2010).

[58] S. J. Glaser, U. Boscain, T. Calarco, C. P. Koch, W. Köckenberger, R. Kosloff, I. Kuprov, B. Luy, S. Schirmer, T. Schulte-Herbrüggen, D. Sugny, and F. K. Wilhelm, Training Schrödinger's cat: Quantum optimal control, Eur. Phys. J. D **69**, 279 (2015).

[59] A. Castro, Optimal control theory for electronic structure methods, in *Handbook of Materials Modeling: Methods: Theory and Modeling*, edited by W. Andreoni and S. Yip (Springer, Cham, Switzerland, 2018), pp. 469–489.

[60] J. P. Palao and R. Kosloff, Quantum Computing by an Optimal Control Algorithm for Unitary Transformations, Phys. Rev. Lett. **89**, 188301 (2002).

[61] Setting the target Floquet modes in the target functional adds an unnecessary extra constraint to the optimization process, if only the energy bands are the target. This constraint could be lifted with a different formulation, written only in terms of the proximity of the generated pseudobands to the target ones. We will develop this idea in a follow-up publication.

[62] D. Kraft, Algorithm 733: Tompfortran modules for optimal control calculations, ACM Trans. Math. Softw. **20**, 262 (1994).

[63] S. G. Johnson, The nlopt nonlinear-optimization package, https://github.com/stevengj/nlopt.

[64] L. S. Pontryagin, V. G. Boltyanskii, R. V. Gamkrelidze, and E. F. Mishechenko, *The Mathematical Theory of Optimal Processes* (Wiley, New York, 1962).

[65] Note that, if the approximation implied by Eq. (13) is not done, the general expression for the gradient would instead be

$$\frac{\partial G}{\partial u_m}(u) = \frac{1}{N_{\mathrm{kps}}} \sum_{\mathbf{k} \in \mathcal{K}} 2 \, \mathrm{Im} \int_0^{t_f} dt \, B_{\mathbf{k}}[u](t) \cdot \left(\frac{\partial H_{\mathbf{k}}(u,t)}{\partial u_m} U_{\mathbf{k}}[u](t) \right).$$

[66] D. J. Tannor and S. A. Rice, Control of selectivity of chemical reaction via control of wave packet evolution, J. Chem. Phys. **83**, 5013 (1985).

[67] S. Shi, A. Woody, and H. Rabitz, Optimal control of selective vibrational excitation in harmonic linear chain molecules, J. Chem. Phys. **88**, 6870 (1988).

[68] A. P. Peirce, M. A. Dahleh, and H. Rabitz, Optimal control of quantum-mechanical systems: Existence, numerical approximation, and applications, Phys. Rev. A **37**, 4950 (1988).

[69] S. Shi and H. Rabitz, Selective excitation in harmonic molecular systems by optimally designed fields, Chem. Phys. **139**, 185 (1989).

[70] R. Kosloff, S. Rice, P. Gaspard, S. Tersigni, and D. Tannor, Wavepacket dancing: Achieving chemical selectivity by shaping light pulses, Chem. Phys. **139**, 201 (1989).

[71] M. Dahleh, A. P. Peirce, and H. Rabitz, Optimal control of uncertain quantum systems, Phys. Rev. A **42**, 1065 (1990).

[72] W. Zhu, J. Botina, and H. Rabitz, Rapidly convergent iteration methods for quantum optimal control of population, J. Chem. Phys. **108**, 1953 (1998).

[73] W. Zhu and H. Rabitz, A rapid monotonically convergent iteration algorithm for quantum optimal control over the expectation value of a positive definite operator, J. Chem. Phys. **109**, 385 (1998).

[74] Y. Maday and G. Turinici, New formulations of monotonically convergent quantum control algorithms, J. Chem. Phys. **118**, 8191 (2003).

[75] J. Somlói, V. A. Kazakov, and D. J. Tannor, Controlled dissociation of I_2 via optical transitions between the X and B electronic states, Chem. Phys. **172**, 85 (1993).

[76] N. Khaneja, T. Reiss, C. Kehlet, T. Schulte-Herbrüggen, and S. J. Glaser, Optimal control of coupled spin dynamics: Design of NMR pulse sequences by gradient ascent algorithms, J. Magn. Reson. **172**, 296 (2005).

[77] S. Machnes, E. Assémat, D. Tannor, and F. K. Wilhelm, Tunable, Flexible, and Efficient Optimization of Control Pulses for Practical Qubits, Phys. Rev. Lett. **120**, 150401 (2018).

[78] T. Caneva, T. Calarco, and S. Montangero, Chopped random-basis quantum optimization, Phys. Rev. A **84**, 022326 (2011).

[79] J. J. W. H. Sørensen, M. O. Aranburu, T. Heinzel, and J. F. Sherson, Quantum optimal control in a chopped basis: Applications in control of Bose-Einstein condensates, Phys. Rev. A **98**, 022119 (2018).

[80] D. H. Dunlap and V. M. Kenkre, Dynamic localization of a charged particle moving under the influence of an electric field, Phys. Rev. B **34**, 3625 (1986).

[81] D. N. Basov, D. N. Basov, and R. D. Averitt, Towards properties on demand in quantum materials, Nat. Mater. **16**, 1077 (2017).